ELSEVIER

Earth and Planetary Science Letters 123 (1994) 95–104

EPSL

A chlorine disinfectant for excess argon released from K-feldspar during step heating

T. Mark Harrison, Matthew T. Heizler [1], Oscar M. Lovera, Chen Wenji, Marty Grove

Department of Earth and Space Sciences and Institute of Geophysics and Planetary Physics, University of California at Los Angeles, 3806 Geology Building, Los Angeles, CA 90024-1567, USA

(Received November 15, 1993; revision accepted March 15, 1994)

Abstract

The release of excess ^{40}Ar ($^{40}Ar_E$) from virtually all alkali feldspars at low temperatures (< 800°C) during $^{40}Ar/^{39}Ar$ step-heating experiments obscures potentially valuable age and thermal history information. We report a method that takes advantage of the differential release of $^{40}Ar_E$ between contiguous isothermal heating steps, due to the decrepitation of fluid inclusions, and which permits derivation of a correction for the contaminating argon. Differences in age and Cl/K between successive temperature pairs commonly yield a single, well-correlated array on a $\Delta(^{40}Ar^*/K)$ versus $\Delta(Cl/K)$ plot that identifies the Cl-correlated composition of $^{40}Ar_E$ ($^{40}Ar_E/Cl$) affecting that sample. Eighteen of the twenty K-feldspar samples we have measured yield a single $^{40}Ar_E/Cl$ component, that varies from 1.1×10^{-3} to 4.2×10^{-6}, making possible recovery of otherwise unobtainable thermochronological information. The upper bound on the $^{40}Ar_E/Cl$ distribution of $\sim 10^{-3}$ may reflect Ar saturation of pore fluids, or the maximum duration between deuteric alteration and cooling below Ar closure in K-feldspar.

1. Introduction

Immediately following determination of the branching ratio for potassium decay, an achievement signaling the birth of K–Ar dating [1], came reports documenting the presence of excess radiogenic ^{40}Ar ($^{40}Ar_E$) in minerals [2]. Over the next two decades, geochronologists attempted with increasing sophistication to overcome this limitation of the K–Ar method [3–6], experiencing only sporadic success. Following development of $^{40}Ar/^{39}Ar$ dating [7], a variant in which a fast neutron reaction creates ^{39}Ar from ^{39}K, the potential of the step-heating method to see through the effects of $^{40}Ar_E$ was explored [8–13]. Because ^{39}Ar is a proxy for the parent (i.e., $^{40}Ar/^{39}Ar$ is implicitly the daughter to the parent ratio, $^{40}Ar/^{40}K$), step heating a single sample can, in principle, yield an isochron array that identifies the isotopic composition of trapped argon. However, the general conclusion of these studies [8–13] was that, apart from providing conservative criteria for the upper age limit of a sample, $^{40}Ar/^{39}Ar$

[PT]

[1] Present Address: New Mexico Bureau of Mines, Socorro, NM 87801, USA.

SSDI 0012-821X(94)00053-2

step-heating studies did not provide a complete solution to the problem of excess argon in minerals. A second point of agreement was that feldspar age spectra containing $^{40}Ar_E$ are characterized by initially old ages that drop rapidly to an apparent plateau, often rising again at higher temperatures [e.g., 11]. In fact, virtually every K-feldspar measured by the $^{40}Ar/^{39}Ar$ method contains, to a greater or lesser degree, $^{40}Ar_E$, obscuring the initial argon release [see 14].

It is now well documented that slowly cooled alkali feldspars contain discrete argon retentivities that are well modeled as a distribution of diffusion domain sizes [15–18]. Because a K-feldspar $^{40}Ar/^{39}Ar$ step-heating experiment yields two distinct sources of information regarding argon retention — the age spectrum and the Arrhenius plot — it is possible to recover the thermal history of a K-feldspar through its *in situ* radiogenic ^{40}Ar ($^{40}Ar_R$) distribution. To establish whether initial low-temperature arrays on Arrhenius plots are meaningful, we adopted the use of paired isothermal steps as part of the laboratory heating schedule. If back-to-back steps at the same temperature yield identical ^{39}Ar diffusivities (D/r^2), it is likely that the activation energy defined by the Arrhenius plot is meaningful. However, if the second isothermal step yields a lower D/r^2 value, the activation energy defined by the low-temperature data may only be apparent [e.g., 19]. In the course of step heating K-feldspars in this fashion, we observed [e.g., 20] that the first step of an isothermal pair was invariably much older than the second (Fig. 1). Subsequently, we recognized that the Cl/K ratio also varied in a similar manner (Fig. 1) and that the two parameters (i.e., apparent age and Cl/K) were intimately related [21].

Of the various sources of reactor-induced argon isotopes, chlorine produces both ^{36}Ar and ^{38}Ar. Cl-derived ^{38}Ar ($^{38}Ar_{Cl}$) is formed by a (n,γ) reaction on ^{37}Cl which produces ^{38}Cl that β^- decays to ^{38}Ar with a half-life of about half an hour [14]. Thus, the ratio of $^{38}Ar_{Cl}$ (determined by subtracting the blank, atmospheric and K-derived contributions from the total ^{38}Ar signal) to $^{39}Ar_K$ is proportional to Cl/K.

Following correction for atmospheric ^{40}Ar ($^{40}Ar_A$), the total radiogenic ^{40}Ar ($^{40}Ar^*$) released during step heating is the sum of both $^{40}Ar_E$ and $^{40}Ar_R$. The ratio $^{40}Ar^*/K$ can be expressed as:

$$^{40}Ar^*/K = (^{40}Ar_E/Cl \cdot Cl/K) + ^{40}Ar_R/K \quad (1)$$

Assuming that $^{40}Ar_E/Cl$ is constant across some interval of gas release, the difference between isotopic results from any two heating steps of equal age (i.e., $\Delta(^{40}Ar_R/K) = 0$) is:

$$\Delta(^{40}Ar^*/K) = ^{40}Ar_E/Cl \cdot \Delta(Cl/K) \quad (2)$$

and thus a plot of log $\Delta(^{40}Ar^*/K)$ versus log $\Delta(Cl/K)$ should yield a linear relationship with an ordinate proportional to the log($^{40}Ar_E/Cl$)

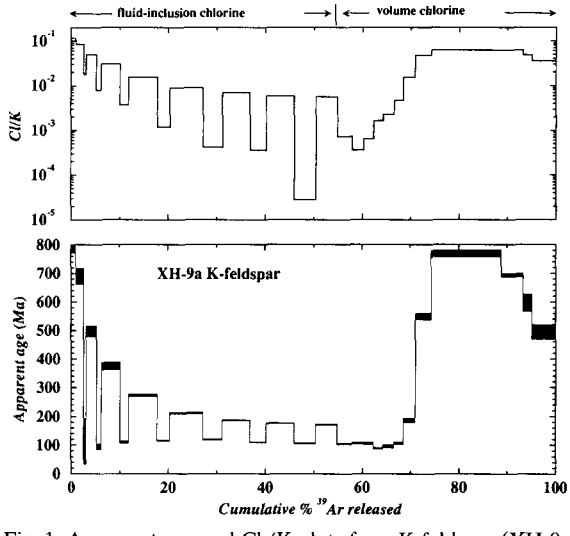

Fig. 1. Age spectrum and Cl/K plots for a K-feldspar (XH-9a) separated from a granite cobble in a Tertiary conglomerate, southern Tibet [see 28]. Although cooling ages in the provenance region, an Andean-type batholith, range from ~100 to 20 Ma, the spectrum yields ages as old as 800 Ma, indicating the presence of excess argon. Following the first heating step at 400°C, two consecutive heating steps were made at each successive temperature up to 850°C. The first of the paired isothermal steps in every case yields both an older age and a higher Cl/K ratio than the second. The difference in age and Cl/K between the contiguous isothermal steps are plotted on a log $\Delta(^{40}Ar^*/K)$ versus log $\Delta(Cl/K)$ plot in Fig. 2b. They yield a linear array that corresponds to an $^{40}Ar_E/Cl = 7.93 \pm 0.11 \times 10^{-5}$. Corrected for the Cl-correlated excess argon, this spectrum yields a plateau age, when between 5% and 70% ^{39}Ar is released, of ~90 Ma. The late released Cl (> 70% ^{39}Ar release) and $^{40}Ar_E$ are interpreted as being volume sited [see 21].

and a slope equal to unity (Fig. 2a). Using paired isothermal heating steps, Harrison et al. [21] documented a relationship between apparent age and Cl/K in the early stages of gas release from a sub-solidus K-feldspar (sample MH-10; see [20,22]) and utilized it to correct the age spectrum for Cl-correlated excess argon. Turner and Wang [23] and Burgess et al. [24] had previously found that Cl-correlated excess argon was released from K-feldspar during *in vacuo* crushing, and Turner and Bannon [25] used an $^{40}Ar_E/Cl$ derived from *in vacuo* crushing to correct for excess argon in quartz and fluorite. However, the two approaches — step heating and *in vacuo* crushing — appear not to access identical features in K-feldspar. For example, the $^{40}Ar_E/Cl$ ratios found by *in vacuo* crushing of MH-10 are three and four times higher, respectively, than that revealed by step heating uncrushed and *in vacuo* crushed splits at low temperatures [21]. Use of the $^{40}Ar_E/Cl$ rela-

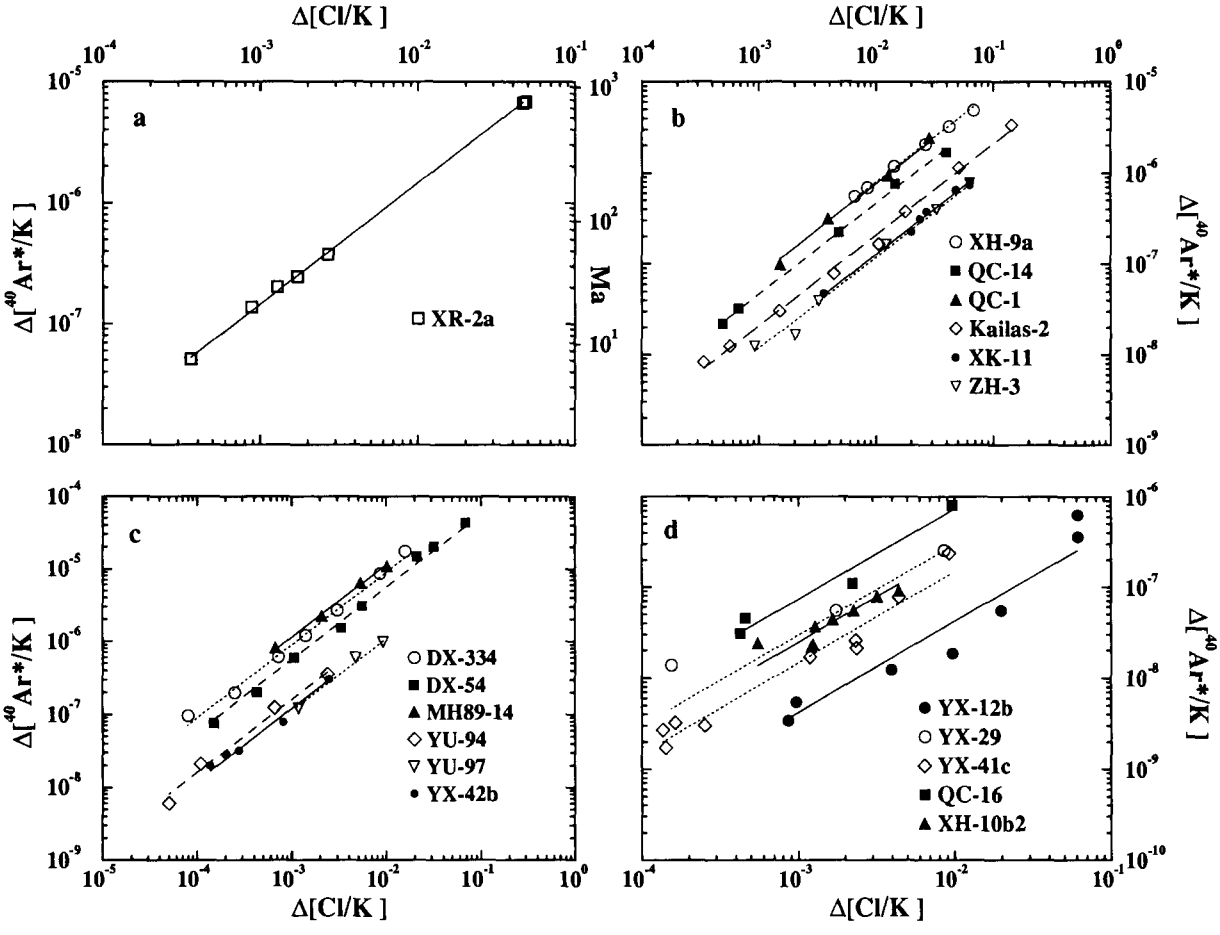

Fig. 2. (a) Log–log plot of $\Delta^{40}Ar^*/K$ versus $\Delta Cl/K$, derived from XR-2a K-feldspar using isothermal steps between 450 and 700°C, which yields $^{40}Ar_E/Cl = 1.45 \pm 0.04 \times 10^{-4}$. The vertical axis on the right shows ages in million years (assuming present day $^{40}K/K$) for the corresponding $\Delta^{40}Ar^*/K$. (b) Log–log plot of $D^{40}Ar^*/K$ versus DCl/K showing results for the Tibetan samples (QC-1, QC-14, Kailas-2, XH-9a, XK-11 and ZH-3) which yield well correlated lines. (c) Log–log plot of $\Delta^{40}Ar^*/K$ versus $\Delta Cl/K$ showing high precision results for the Dabie Shan (DX-334 and DX-54), Jiangsu (MH89-14), and Ailao Shan (YU-94, YU-97 and YX-42b) samples. DX-54 shows the greatest spread in $\Delta^{40}Ar^*/K$ of all samples, yielding a constant $^{40}Ar_E/Cl$ ratio of $5.58 \pm 0.06 \times 10^{-4}$ for age differences that vary from 10 to 2900 Ma. (d) Log–log plot of $\Delta^{40}Ar^*/K$ versus $\Delta Cl/K$ showing the more weakly correlated results (YX-12b, YX-29, YX-41c, QC-16 and XH-10B2).

tionship obtained for MH-10 from *in vacuo* crushing would result in a substantial overcorrection (i.e., yield negative ages) of most low-temperature step-heating ages [21]. This difference may be due, in part, to sampling of grain boundary-held $^{40}Ar_E$ by the *in vacuo* crushing method, which might have been lost prior to the step-heating analysis due to the preliminary heat treatment at ~ 300°C we employ to melt the tin foil sample packet. Furthermore, note that not all of the Cl-derived argon is lost from K-feldspar during low-temperature heating. A substantial fraction (typically > 60%) is liberated from lattice sites at high temperatures (> 950°C), apparently by volume diffusion [21] (Fig. 1). Thus, it is not surprising that the *in vacuo* crushing and step-heating methods could access different reservoirs of Ar and Cl in the same K-feldspar. Our point is not to suggest that step heating yields the better bulk sample estimate of $^{40}Ar_E/Cl$. Rather, that it produces the $^{40}Ar_E/Cl$ that is specifically relevant to age correction of low-temperature step-heating results.

Excess argon-to-chlorine ratios ($^{40}Ar_E/Cl$) derived from 20 basement K-feldspars are presented in Table 1. We conclude that the presence

Table 1
Rock type, K-feldspar $^{40}Ar/^{39}Ar$ age, sample location and K-feldspar $^{40}ArE/Cl$ results

sample	rock type	Age (Ma)	Latitude/Longitude	$^{40}Ar_E/Cl$ (±1σ)	Ref.
Red River shear zone, Ailao Shan, Yunnan Province					
YU-94	sheared gneiss	17-20	24°27.0'N/101°14.9'E	$1.59 \pm 0.23 \times 10^{-4}$	[42]
YU-97	sheared gneiss	17-20	24°27.0'N/101°14.9'E	$1.10 \pm 0.10 \times 10^{-4}$	[42]
YX-12b	sheared gneiss	20-22	23°35.1'N/101°56.5'E	$4.2 \pm 0.4 \times 10^{-6}$	[42]
YX-16a	mylonite	19-22	23°52.4'N/101°40.0'E	$\sim 10^{-4}$	[42]
YX-29	sheared gneiss	19-21	23°47.0'N/101°42.2'E	$2.96 \pm 0.12 \times 10^{-5}$	[42]
YX-41c	mylonite	17-22	24°9.7'N/101°27.1'E	$1.49 \pm 0.25 \times 10^{-5}$	[42]
YX-42b	sheared gneiss	19-21	24°9.7'N/101°27.1'E	$1.20 \pm 0.10 \times 10^{-4}$	[42]
Bixiling batholith, southern Dabie Shan, Anhui Province					
DX-334	mylonite	95-165	30°40'N/116°20'E	$8.87 \pm 0.16 \times 10^{-4}$	
DX-54	gneiss	110-290	30°40'N/116°20'E	$5.58 \pm 0.06 \times 10^{-4}$	
Tanlu fault zone, Shuanghu village, northern Jiangsu Province					
MH89-14	gneiss	125-200	34°35'N/118°35'E	$1.13 \pm 0.06 \times 10^{-3}$	[43]
Southern Tibet					
Kailas-2	granodiorite	30-39	31°13'N/81°24'E	$2.07 \pm 0.08 \times 10^{-5}$	
QC-1	granodiorite	5-15	30°12.3'N/90°24.4E	$7.6 \pm 0.4 \times 10^{-5}$	[44]
QC-14	granodiorite	7-12	30°19.4'N/90°31.1'E	$4.6 \pm 0.3 \times 10^{-5}$	[44]
QC-16	granodiorite	5-10	30°18.3'N/90°33.5'E	$7.3 \pm 2.0 \times 10^{-5}$	[44]
XH-9a	granitoid cobble	~90	29°21.1'E/88°17.8'E	$7.93 \pm 0.11 \times 10^{-5}$	[28]
XH-10b2	andesite dyke	17	29°20.1'E/88°31.0'E	$2.47 \pm 0.45 \times 10^{-5}$	[28]
XK-11	dacitic sill	18	29°18.6'E/88°48.4'E	$1.27 \pm 0.04 \times 10^{-5}$	[28]
XR-2a	granodiorite	9-60	29°18.3'N/90°21.8'E	$1.45 \pm 0.04 \times 10^{-4}$	[27]
ZH-3	granodiorite	20-27	29°15.3'N/91°53.8'E	$1.26 \pm 0.07 \times 10^{-5}$	[28]
ZH-2b	sheared granitoid	26-28	29°15.3'N/91°53.8'E	$< 2 \times 10^{-5}$	[28]

of a single $^{40}Ar_E/Cl$ component in these samples is the rule rather than the exception and suggest that our approach has wide applicability in correcting the low-temperature portion of K-feldspar age spectra for excess argon. Because the initial gas release from $^{40}Ar/^{39}Ar$ age spectra is almost always disregarded for this reason, an important implication of these results is that K-feldspar thermochronometry can routinely be extended to much lower temperatures (ca. 150°C) than previously accessible.

2. $^{40}Ar_E/Cl$ and thermal histories

Between July 1992 and August 1993, we performed $^{40}Ar/^{39}Ar$ step-heating measurements on

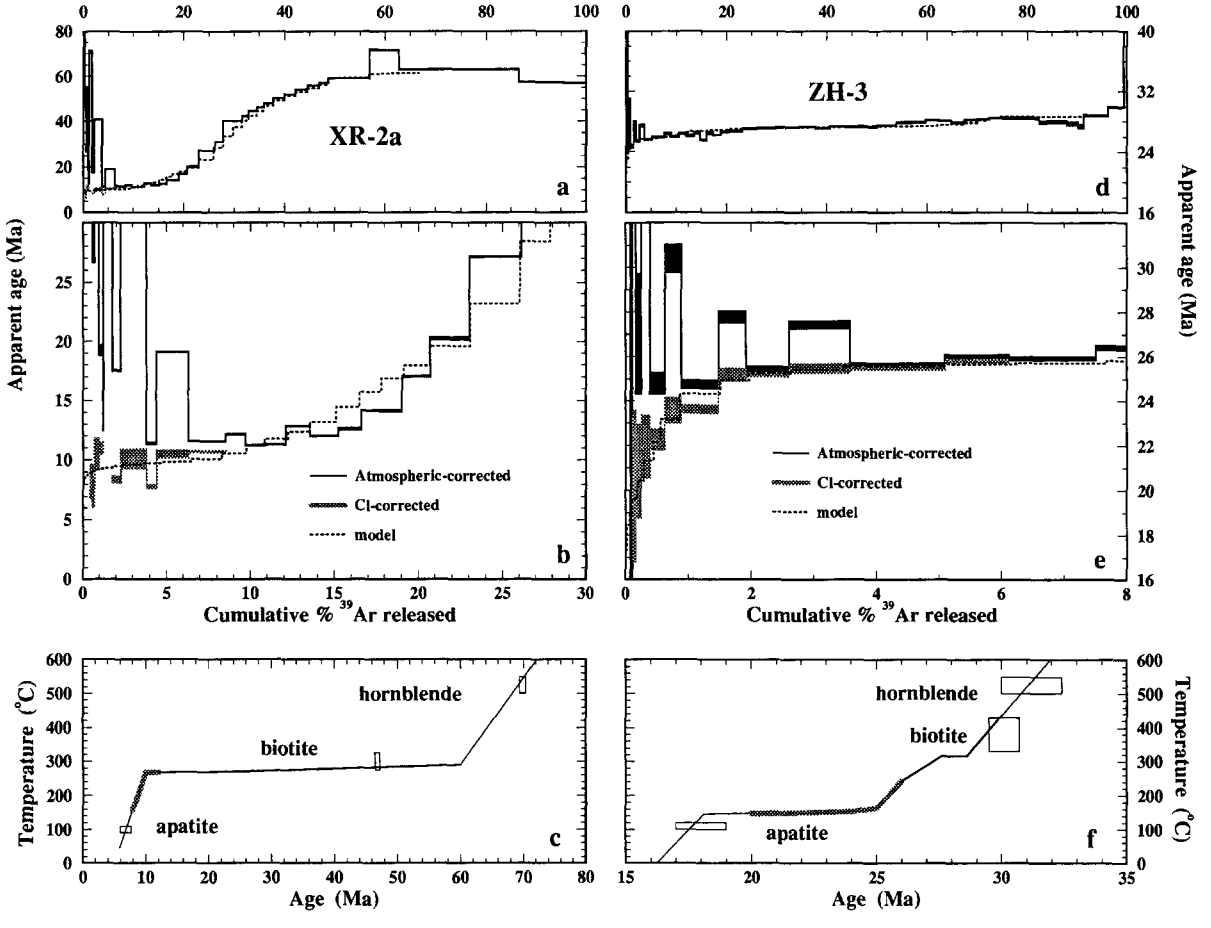

Fig. 3. (a) $^{40}Ar/^{39}Ar$ age spectrum for XR-2a K-feldspar. (b) Expanded portion of (a) showing the atmospheric-corrected data (black areas), Cl-corrected data (stippled areas) and model age spectrum (dashed line) predicted from the thermal history shown in (c). (c) Proposed thermal history for XR-2a showing portion constrained by the K-feldspar results (thick line = following atmospheric correction; stippled line = following Cl correction) along with apatite fission track (see text) and $^{40}Ar/^{39}Ar$ hornblende (69.9 ± 0.5 Ma) and biotite (46.0 ± 0.2 Ma) ages and closure temperatures [14]. (d) $^{40}Ar/^{39}Ar$ age spectrum for ZH-3 K-feldspar. (e) Expanded portion of (d) showing the atmospheric-corrected data (black areas), Cl-corrected data (stippled areas), and model age spectrum (dashed line) predicted from the thermal history shown in (f). (f) Proposed thermal history for ZH-3 showing portion constrained by the K-feldspar results (thick line = following atmospheric correction; stippled line = following Cl correction) along with apatite fission track (see text) and $^{40}Ar/^{39}Ar$ hornblende (31.6 ± 1.5 Ma) and biotite (30.1 ± 0.5 Ma) ages and closure temperatures [14].

20 igneous and metamorphic K-feldspar samples using paired isothermal steps [see 16,20 for analytical details] in the low-temperature portion of the gas release. We found clear correlations between $\Delta(^{40}Ar^*/K)$ and $\Delta(Cl/K)$ (shown in Fig. 2 on log–log plots) in 18 out of the 20 samples and only weak correlations in the other two (samples YX-16a and ZH-2b). The derived $^{40}Ar_E/Cl$ ratios, which vary from 1.13×10^{-3} to 4.2×10^{-6}, are listed along with calculated regression uncertainties in Table 1. Although two-axis logarithmic plots are useful to display data that vary by up to three orders of magnitude, a linear array on this kind of plot requires that rigorous conditions be satisfied. A linear relationship plots as a curve on a log–log plot in all instances except when, as in our case, the intercept is zero. Also, note from Eq. (2) that the slope of the line in the log–log plot is constrained to be unity, therefore reducing the degree of freedom in the least-square fitting to only one parameter — the ordinate ($\log(^{40}Ar_E/Cl)$). Thus, it is remarkable that 13 of the 18 results (Fig. 2a–c) conform to unit slopes with associated uncertainties that are at the level of experimental error of the measured isotopic ratios. This indicates that, at the resolution of a few to several percent uncertainty, the low-temperature portion of gas release is affected by only a single source of $^{40}Ar_E$ that is Cl-correlated. The remaining five results (Fig. 2d), while less clearly containing only a single component, still have an average uncertainty of only $\pm 15\%$.

The method by which we produce these plots and apply their results are illustrated using K-feldspar XR-2a (Fig. 2a). This sample is from the Yadong–Gulu rift, a Neogene graben in southern Tibet thought to represent tectonic collapse in response to the Tibetan plateau attaining maximum sustainable elevation [see 26 and references therein]. The K-feldspar was heated in 50°C increments, between 450° and 750°C, with back-to-back steps measured at each temperature (and three steps at 500°C). The related portion of the age spectrum (0–8% ^{39}Ar released) is characterized by a saw-toothed pattern, with ages ranging between 833 and 11.4 Ma (Fig. 3a), with the first heating step yielding both a significantly higher age and Cl/K than the subsequent step. Between 8% and 60% ^{39}Ar release, the spectrum climbs in a smooth fashion to an age of ~ 60 Ma. $^{40}Ar^*/K$ values for each heating step were calculated from the argon isotope results using a standard atmospheric correction [23]. Cl/K values were calculated through the relationship $Cl/K = {}^{38}Ar_{Cl}/{}^{39}Ar_K \cdot 0.277$ [see 21]. Each set of ratios were then subtracted from their isothermal step counterparts to yield seven $\Delta(^{40}Ar^*/K)$ and $\Delta(Cl/K)$ pairs spanning two orders of magnitude (Fig. 2a). In general, these ratios progressively decrease as temperature is raised. The excellent fit of the log $\Delta(^{40}Ar^*/K)$ and log $\Delta(Cl/K)$ ratios to a straight line of unit slope requires that all $^{40}Ar_E$ be Cl-correlated. The sole exception to this conclusion would be the case where an $^{40}Ar_E$ component is uniformly (to better than a few percent) distributed throughout the sample. We judge the occurrence of this kind of distribution in a slowly cooled mineral to be unlikely.

Using the $^{40}Ar_E/Cl$ derived from this plot (Fig. 2a) of $1.45 \pm 0.04 \times 10^{-4}$ (Table 1), an $^{40}Ar_E$ age correction (i.e., $^{40}Ar_R/K = {}^{40}Ar^*/K - [(^{40}Ar_E/Cl) \cdot Cl/K]$) was then applied to each step over the first 8% of ^{39}Ar release (Fig. 3b). Errors in both $^{40}Ar_E/Cl$ and age were propagated through the calculations. Due to the large magnitude of the correction (up to 99%), ages over the first 0.5% of ^{39}Ar release have very high uncertainties. However, the subsequent ten steps, atmosphere-corrected to ages ranging from 74 to 11.4 Ma, Cl correct to an age of 9 ± 1 (1σ) Ma.

Using the experimentally derived Arrhenius and distribution parameters [15–17], an excellent model fit to the original age spectrum (Fig. 3a) is obtained, assuming an essentially isothermal history between 60 and 10 Ma (Fig. 3c). The portion of the spectrum previously obscured by $^{40}Ar_E$ (0–8% ^{39}Ar released) is consistent with rapid cooling, beginning at temperature of 270°C at 10–9 Ma and proceeding at a rate of about 100°C/m.y. (Fig. 3b). An apatite fission track age of 7 ± 1 Ma [26] from within the graben, but several kilometers further east, is consistent with this history. The onset of cooling at 9 ± 1 Ma may be geologically significant, because thermal history data from the detachment fault bounding the western side of the graben indicate that signifi-

cant motion and concomitant cooling began at 8 ± 1 Ma [26].

The rapid cooling experienced by XR-2a makes it ideal for correction by our method, because it accords closely to the model assumptions; specifically, that $\Delta(^{40}Ar_R/K) = 0$ (i.e., the radiogenic age is constant). Note, however, that $\Delta^{40}Ar^*/K$ and $\Delta Cl/K$ are generally large relative to the magnitude of an age gradient ($\Delta^{40}Ar_R/K$) across a small interval of ^{39}Ar release. Thus, the calculations tend to be insensitive to small differences in this parameter, permitting thermal histories to be obtained for cases involving slow cooling. An example of this cooling style is given by the ZH-3 K-feldspar, a granodiorite sample from the hanging wall of the Gangdese thrust in southern Tibet [26,28]. The age spectrum of ZH-3 K-feldspar is characterized by a saw-toothed pattern over the first 6% of ^{39}Ar release (Fig. 3d). Its $\Delta(^{40}Ar^*/K)$ and $\Delta(Cl/K)$ data are well correlated and yield an $^{40}Ar_E/Cl$ ratio of $1.26 \pm 0.07 \times 10^{-5}$ (Table 1, Fig. 2b). This value is indistinguishable from a less precise duplicate measurement of $^{40}Ar_E/Cl = 1.38 \pm 0.24 \times 10^{-5}$. Applying the Cl correction to the first 6% of ^{39}Ar release results in a substantially modified spectrum, which is characterized by a monotonic increase in ages between 20.2 ± 3.4 and 25.8 ± 0.1 Ma (Fig. 3e). Diffusion modeling of this portion of the spectrum [15–17,28] indicates that slow cooling (~ 3°C/m.y.) continued between 25 and 20 Ma, when a temperature of 150°C was reached (Fig. 3f). This history is also consistent with the coexisting apatite fission track age, which indicates that a temperature of 110 ± 10°C was reached at 18 ± 1 Ma [28].

The remaining sixteen samples for which we obtained $^{40}Ar_E/Cl$ relationships also yield sensible age spectra following correction for Cl-correlated $^{40}Ar_E$, but lack the independent constraint on the low-temperature thermal history provided by apatite fission track ages. Release of $^{40}Ar_E$ has largely precluded extracting thermal history information from K-feldspar age spectra for temperatures much below 200°C [15–17]. Depending on the degree of excess argon contamination and the argon retentivity, the portion of the K-feldspar age spectrum now recoverable using the Cl correction corresponds, in some cases, to temperatures as low as 130°C. Not only does this permit near overlap with apatite fission track results, but should significantly enhance several applications of K-feldspar thermochronometry, such as basin thermal histories and denudation studies [14].

3. The significance of the $^{40}Ar_E/Cl$ distribution

On the basis of TEM and scanning ion imagery, Harrison et al. [21] concluded that the source of the disproportionate release of Cl-correlated excess argon from the first of the two isothermal steps was decrepitation of fluid inclusions. Very little of this component was released during the second step because the potential for decrepitation at that temperature had already been largely realized. We stress that, in the basement K-feldspars we have analyzed, these micropores are rare (typically < 1 vol%) and contain an exceedingly small portion of the total sample potassium (typically $\sim 0.1\%$) and thus do not influence the calculation of thermal histories [20–22]. Their principal significance to thermochronometry is the fact that they carry $^{40}Ar_E$.

Many factors (size, shape, fluid density and composition, and heating rate) control the tensile strength of fluid inclusions and the relationship between the temperatures of decrepitation and formation is not entirely clear [29,30]. The greatest release of $^{40}Ar_E$ is at temperatures of 400–450°C. This is similar to temperatures proposed by Ferry [31] for the alteration of alkali feldspar by dissolution–reprecipitation, the process thought by Parsons et al. [32] to be responsible for the creation of microporosity in alkali feldspars. Although progressively smaller amounts of Cl-correlated argon continue to be released at temperatures up to ~ 750°C, much of this gas is probably derived from nanometer-scale pores formed during decrepitation of the larger inclusions [20–22]. Formation of such secondary inclusions without significant fractionation of argon isotopes may explain why $\Delta(^{40}Ar^*/K)$ versus $\Delta(Cl/K)$ plots are so highly correlated.

Speculations regarding the significance of the

$^{40}Ar_E/Cl$ ratios are complicated by the inability to determine precisely the Cl concentration in the released fluids and the paucity of solubility data for rare gases. Due to the fact that the feldspar inclusions are generally sub-microscopic, it is not possible for us to estimate their salinity from homogenization studies [29]. Although there is a good deal of information regarding the solubility of argon in brines at relatively low temperatures [33,34], studies at elevated P–T conditions have only been undertaken using pure water [e.g., 35]. Because the presence of dissolved electrolytes is known to have a significant influence on the solubilities of rare gases in water ('the salting effect'), direct application of existing experimental studies to mid-crustal conditions is problematic.

The range in $^{40}Ar_E/Cl$ from the 18 results from 1.1×10^{-3} to 4×10^{-6} (Table 1) is remarkably similar to the span of values reported for K-feldspar in the literature (1.0×10^{-3} to 3×10^{-6}) [21,23,24,36]. Within the combined data set ($n = 25$), there are a similar number of $^{40}Ar_E/Cl$ values in the range 10^{-5} to 10^{-4} ($n = 11$) as there are between 10^{-4} and 10^{-3} ($n = 12$). However, the distribution has an abrupt cutoff at $^{40}Ar_E/Cl = 10^{-3}$ (Fig. 4). Although four values define the upper bound at $1.0 \pm 0.1 \times 10^{-3}$, no higher $^{40}Ar_E/Cl$ values, or for that matter $(Ar_E + Ar_A)/Cl$ values, have been reported from K-feldspars or other mineral hosts [25,37,38]. Although most of the K-feldspar results are sufficiently radiogenic to ignore other contributions, the datum of Burgess and Parsons [36] ($^{40}Ar_E/Cl \approx 2.6 \times 10^{-6}$) is dominated by $^{40}Ar_A$, due to rock interaction with meteoric water. The highest value of $(^{40}Ar_E + ^{40}Ar_A)/Cl$ from this sample of $1.04 \pm 0.07 \times 10^{-3}$ is identical to the upper bound of the $^{40}Ar_E/Cl$ distribution (Fig. 4). Differing abundances of dissolved argon and chlorine in crustal fluids (due to variations in temperature, pressure and source characteristics) would be expected to produce a very broad range of $^{40}Ar_E/Cl$ values. This distribution might also be expected to have an upper limit corresponding to Ar saturation in Cl-rich solutions under mid-crustal environmental conditions. Apparent termination of the distribution at an $^{40}Ar_E/Cl \approx 10^{-3}$ might reflect Ar saturation, although we cannot rule out statistical vagaries of a still relatively small data set.

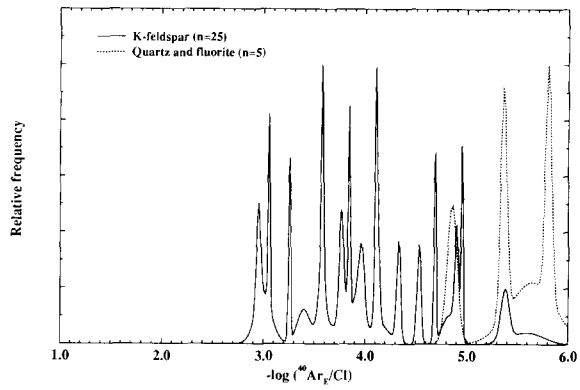

Fig. 4. Probability plot showing the relative frequency of occurrence of $^{40}Ar_E/Cl$ in step heating [20, Table 1] and *in vacuo* crushing [21,23,24,36] studies of K-feldspar (solid line). The plot is derived by superimposing the gaussian distributions for all 25 ratios and their associated uncertainties. $^{40}Ar_E/Cl$ results from *in vacuo* crushing or laser fusion of quartz and fluorite (dotted line) from five mineralized districts [25,37,38] are also shown. Although the distribution of $^{40}Ar_E/Cl$ values is relatively uniform between 10^{-5} and 10^{-3}, no values have been reported that significantly exceed the latter value. The upper bound of this distribution may represent either argon saturation in crustal brines or an upper limit on the time between deuteric alteration and cooling below Ar closure in K-feldspar.

Assuming, for the purposes of calculation, a Cl concentration of 2 wt.% in the trapped fluid, probably correct to within a factor of five [23,36,38], an Ar/Cl of 10^{-3} corresponds to a mole fraction of dissolved argon (x_{Ar}) of $\sim 10^{-5}$. The mixing behavior of Ar in pure water at the conditions of interest ($\sim$ 2–3 kbar, $\sim$ 350–450°C) is complex [39,40] but suggests an x_{Ar} of about 10^{-1}. The tremendous disparity between these two estimates may reflect a reduction in Ar solubility due to the salting effect. Alternatively, the apparent upper limit of $x_{Ar} \approx 10^{-5}$ could simply reflect the maximum time available between formation of the microporosity and cooling below Ar closure in K-feldspar. If any fluid-filled crack in a crustal rock could achieve argon saturation due to local radiogenic production, it would be one hosted by K-feldspar. For example, assuming present day isotopic abundances and average values for K (3%) and Cl (180 ppm) in a granodiorite

[41], the time (Δt) required to achieve a bulk rock $^{40}Ar_R/Cl = 10^{-3}$ would be $\Delta t = \lambda^{-1} \ln [1 + (^{40}Ar_R/Cl) + (Cl/K) + 9 \times 10^4] = 780$ m.y. However, a K-feldspar containing 15% K and 50 ppm Cl [21] would reach $^{40}Ar_R/Cl = 10^{-3}$ in only ~ 50 m.y. A water-filled porosity of 0.5% [22], capturing the entire $^{40}Ar_R$ production of an encompassing K-feldspar, would, likewise, yield an x_{Ar} of $\sim 10^{-5}$ in about 40 m.y. In general, K-feldspars yielding the highest $^{40}Ar_E/Cl$ ratios are characterized by protracted thermal histories, typically in excess of 100 m.y. between formation age and cooling below Ar closure in K-feldspar. We cannot, at present, select between these two hypotheses but have begun hydrothermal synthesis of fluid inclusions in quartz under mid-crustal P–T conditions in Ar-saturated brines. Argon isotopic measurements of the irradiated products should give us a clearer picture of the effect of salinity on Ar solubility in crustal fluids. Likewise, measurement of K-feldspars from slowly cooled Precambrian terranes are being undertaken to examine the durability of the upper limit in the $^{40}Ar_E/Cl$ distribution.

4. Conclusions

The differential release of Cl-correlated $^{40}Ar_E$ from contiguous isothermal heating steps, apparently due to thermal decrepitation of sub-microscopic fluid inclusions, provides the basis for a correction to be applied to the age spectrum. Successive isothermal temperature pairs plotted on a $\Delta(^{40}Ar^*/K)$ versus $\Delta(Cl/K)$ diagram commonly yield a single, well correlated array that is proportional to $^{40}Ar_E/Cl$. Eighteen out of twenty K-feldspars analyzed by $^{40}Ar/^{39}Ar$ step heating yield $^{40}Ar_E/Cl$ values that vary from 1.1×10^{-3} to 4.2×10^{-6}. The apparent cutoff in the $^{40}Ar_E/Cl$ distribution at $\sim 10^{-3}$ may either reflect Ar saturation in mid-crustal fluids or an upper limit on the time between deuteric alteration and cooling below Ar closure in K-feldspar. By identifying the Cl-correlated composition of $^{40}Ar_E$ and applying the resulting age correction to the early steps, the low-temperature portion of thermal histories appears to be routinely recoverable from K-feldspar $^{40}Ar/^{39}Ar$ results.

Acknowledgments

Support for this research was derived from a grant from the Office of Basic Energy Research, Department of Energy. Samples were obtained with the assistance of W.S.F. Kidd, F.J. Ryerson, P. Copeland, A. Yin, P.H. Leloup and Li Qi. We thank Ray Burgess, Craig Manning, Kevin McKeegan, Jeff Fillipone and anonymous reviewers for constructive reviews.

References

[1] G.W. Wetherill, Radioactivity of potassium and geologic time, Science 126, 545–549, 1957.
[2] P.E. Damon and J.L. Kulp, Excess helium and argon in beryl and other minerals, Am. Mineral. 43, 433–459, 1957.
[3] J.F. Evernden and J.R. Richards, Potassium–argon ages at Broken Hill, Australia, Nature 192, 446, 1961.
[4] I. McDougall and D.H. Green, Excess radiogenic argon in pyroxene and isotopic ages on minerals from Norwegian eclogites, Nor. Geol. Tidsskr. 44, 183–196, 1964.
[5] A.W. Laughlin, Excess radiogenic argon in pegmatite minerals, J. Geophys. Res. 74, 6684–6690, 1969.
[6] J.C. Roddick and E. Farrar, High initial argon ratios in hornblendes, Earth Planet. Sci. Lett. 12, 208–214, 1971.
[7] G. Merrihue and G. Turner, Potassium–argon dating by activation with fast neutrons, J. Geophys. Res. 71, 2852–2857, 1966.
[8] M.A. Lanphere and G.B. Dalrymple, A test of the $^{40}Ar/^{39}Ar$ age spectrum technique on some terrestrial minerals, Earth Planet. Sci. Lett. 12, 359–372, 1971.
[9] I. Kaneoka, Investigation of excess argon in ultramafic rocks form the Kola Peninsula by the $^{40}Ar/^{39}Ar$ method, Earth Planet. Sci. Lett. 22, 145–156, 1974.
[10] D.E. Seidemann, An $^{40}Ar/^{39}Ar$ age spectrum for a cordierite-bearing rock: isolating the effects of excess radiogenic ^{40}Ar, Earth Planet. Sci. Lett. 33, 268–272, 1976.
[11] M.A. Lanphere and G.B. Dalrymple, Identification of excess ^{40}Ar by the $^{40}Ar/^{39}Ar$ age spectrum technique, Earth Planet. Sci. Lett. 32, 141–148, 1976.
[12] E.K. Jessberger, Comment on "Identification of excess ^{40}Ar by the $^{40}Ar/^{39}Ar$ age spectrum technique", Earth Planet. Sci. Lett. 37, 167–168, 1977.
[13] M.A. Lanphere and G.B. Dalrymple, Reply to comment by E.K. Jessberger, Earth Planet. Sci. Lett. 37, 169–171, 1977.
[14] I. McDougall and T.M. Harrison, Geochronology and Thermochronology by the $^{40}Ar/^{39}Ar$ Method, 212 pp., Oxford Univ. Press, New York, 1988.
[15] O.M. Lovera, F.M. Richter and T.M. Harrison, $^{40}Ar/^{39}Ar$ thermochronometry for slowly cooled samples having a

distribution of diffusion domain sizes, J. Geophys. Res. 94, 17917–17935, 1989.
[16] T.M. Harrison, O.M. Lovera and M.T. Heizler, $^{40}Ar/^{39}Ar$ results for multi-domain samples with differing activation energy, Geochim. Cosmochim. Acta 55, 1435–1448, 1991.
[17] O.M. Lovera, F.M. Richter and T.M. Harrison, Diffusion domains determined by ^{39}Ar release during step heating, J. Geophys. Res. 96, 2057–2069, 1991.
[18] P.K. Zeitler, Argon diffusion in partially degassed alkali feldspar: insights from $^{40}Ar/^{39}Ar$ analyses, Chem. Geol. (Isot. Geosci. Sect.) 65, 167–181, 1987.
[19] M.T. Heizler and T.M. Harrison, The heating duration and provenance ages of rocks in the Salton Sea Geothermal Field, southern California, J. Volcanol. Geotherm. Res. 46, 73–97, 1991.
[20] O.M. Lovera, M.T. Heizler and T.M. Harrison, Argon diffusion domains in K-feldspar II: Kinetic properties of MH-10, Contrib. Mineral. Petrol. 113, 381–393, 1993.
[21] T.M. Harrison, M.T. Heizler and O.M. Lovera, In vacuo crushing experiments and K-feldspar thermochronometry, Earth Planet. Sci. Lett. 117, 169–180, 1993.
[22] J.D. Fitz Gerald and T.M. Harrison, Argon diffusion domains in K-feldspar I: Microstructures in MH-10, Contrib. Mineral. Petrol. 113, 367–380, 1993.
[23] G. Turner and S. Wang, Excess argon, crustal fluids and apparent isochrons from crushing K-feldspar, Earth Planet. Sci. Lett. 110, 193–211, 1992.
[24] R. Burgess, S.P Kelley, I. Parsons, F.D.L. Walker and R.H. Worden, $^{40}Ar-^{39}Ar$ analysis of perthite microstructures and fluid inclusions in alkali feldspars from the Klokken syenite, South Greenland, Earth Planet. Sci. Lett. 109, 147–167, 1992.
[25] G. Turner and M.P. Bannon, Argon isotope geochemistry of inclusion fluids from granite-associated mineral veins in southwest and northeast England, Geochim. Cosmochim. Acta 56, 227–243, 1992.
[26] T.M. Harrison, P. Copeland, W.S.F. Kidd and A. Yin, Raising Tibet, Science 255, 1663–1670, 1992.
[27] P. Copeland, Y. Pan, T.M. Harrison, W.S.F. Kidd and M. Roden, Thermal evolution of the Gangdese batholith, southern Tibet: A history of episodic unroofing, Tectonics, in press, 1994.
[28] A. Yin, T.M. Harrison, F.J. Ryerson, W. Chen, W.S.F. Kidd and P. Copeland, Tertiary structural evolution of the Gangdese thrust system, southeastern Tibet, J. Geophys. Res., in press, 1994.
[29] E. Roedder, Fluid Inclusions, Reviews in Mineralogy Vol. 12, 644 pp., Mineral. Soc. Am., 1984.
[30] R.J. Bodnar, P.R. Binns and D.L. Hall, Synthetic fluid inclusions — VI. Quantitative evaluation of the decrepitation behavior of fluid inclusions in quartz at one atmosphere confining pressure, J. Metamorph. Geol. 7, 229–242, 1989.
[31] J.M. Ferry, Hydrothermal alteration of Tertiary igneous rocks from the Isle of Skye, northwest Scotland. II Granites, Contrib. Mineral. Petrol. 91, 283–304, 1985.
[32] I. Parsons, D.C. Rex, P. Guise and A.N. Halliday, Argon loss by alkali feldspars, Geochim. Cosmochim. Acta 52, 1097–1112, 1988.
[33] M. Ozima and F.A. Podosek, Noble Gas Geochemistry, 367 pp., Cambridge Univ. Press, London, 1983.
[34] S.P. Smith and B.M. Kennedy, The solubility of noble gases in water and in NaCl brine, Geochim. Cosmochim. Acta 47, 503–515, 1983.
[35] R. Crovetto, R. Fernández-Prini and M.L. Japas, Solubilities of inert gases and methane in H_2O and in D_2O in the temperature range of 300 to 600 K, J. Chem. Phys. 76, 1077–1087, 1982.
[36] R. Burgess and I. Parsons, Argon and halogen geochemistry of hydrothermal fluids in the Loch Ainort granite, Isle of Skye, Scotland, Contrib. Mineral. Petrol., in press, 1994.
[37] S.P. Kelley, G. Turner, A.W. Butterfield and T.J. Shepherd, The source and significance of argon isotopes in fluid inclusions from areas of mineralization, Earth Planet. Sci. Lett. 79, 303–318, 1986.
[38] J.K. Bölke and J.J. Irwin, Brine history indicated by argon, krypton, chlorine, bromine, and iodine analyses of fluid inclusions from the Mississippi Valley type lead–fluorite–barite deposits at Hansonburg, New Mexico, Earth Planet. Sci. Lett. 110, 51–66, 1992.
[39] E.L. Shock, H.C. Helgeson and D.A. Sverjensky, Calculation of the thermodynamic and transport properties of aqueous species at high pressures and temperatures: Standard partial molal properties of inorganic neutral species, Geochim. Cosmochim. Acta 53, 2157–2183, 1989.
[40] H. Lentz and E.U. Franck, Das system wasser–argon bei hohen drucken und temperaturen, Ber. Bunsen-Ges. Phys. Chem. 73, 28–35, 1969.
[41] R.M. Garrels and F.T. MacKenzie, Evolution of Sedimentary Rocks, W.W. Norton, New York, 1971.
[42] T.M. Harrison, F.J. Ryerson, P.H. Leloup, C. Wenji, P. Tapponnier, O.M. Lovera, U. Schärer and R. Lacassin, Thermal evolution of the Red River/Ailao Shan shear zone, in: The Tectonics of Asia, A. Yin and T.M. Harrison, eds., Rubey Vol. IX, submitted, 1994.
[43] W. Chen, T.M. Harrison, M.T. Heizler, L. Ruoxin, M. Bolin and L. Jiliang, The cooling history of a melange zone in North Jiangsu–South Shandong region: evidence from multiple diffusion domain $^{40}Ar-^{39}Ar$ thermal geochronology, Acta Petrol. Sinica 8, 1–17, 1992.
[44] T.M. Harrison, P. Copeland, P. Yun, W.S.F. Kidd and O.M. Lovera, The Nyainqentanghla shear zone: implications for Tibetan plateau uplift and onset of the Asian monsoon, in prep., 1994.